Slip effect on Magnetohydrodynamic boundary layer flow of nanofluid over an stretching sheet with thermal radiation and thermal convective boundary condition ⋆

Abstract

The objective of the current analysis is to study the influence of MHD on flow of an ethylene glycol-based nanofluid containing copper nanoparticles through a exponential stretching sheet. Several parameters including Dufour, thermal radiation, Magnetohydrodynamic (MHD), and Eckart number, were investigated for their impacts on fluid flow, heat and mass transfer profiles, and thermal convective boundary conditions, while Navier velocity slip was also considered. The basic PDEs are transformed into nondimensional ODEs using appropriate transformations and numerically characterized by bvp4c. The graphs examine the influence of relevant parameters on heat and mass transfer profiles. The velocity profile decrease with slip effect. As the Biot number increased, the thermal layer became thicker. The Nusselt number are the decline functions of magnetic field, Eckert number and Brownian diffusion but the local Sherwood number enhanced with these parameters. The Nusselt number intensifies with radiation parameter R_d, slip parameter λ and Biot numberB_i. The temperature and concentration profiles rises with increase in N_t.

Keywords: Nanofluid, Convective boundary conditions, Thermal radiation, Slip effect, fluid, bvp4c

2010 MSC: 00-01, 99-00

1. Introduction

Nanofluid is a novel technique of improving heat transfer properties, because of its wide range of applications in industry and technology, the research of boundary layer flow and heat transfer over a stretching surface has had a lot of success in recent years. Polymer extrusion, copper wire drawing, continuous stretching of plastic films, artificial fibres, hot rolling, wire drawing, glass fibre, metal extrusion, and metal spinning are just a few of these applications.The thermal conductivity of the working fluid determines the efficiency of heat transfer. Thus, a new class of engineering fluid called nanofluid is formed by increasing the thermal conductivity of working fluids such as water, ethyl glycol, and oil by floating a small proportion of nanoparticle (such as Cu, Ag, TiO2, and Al2O3) in it [1]. Using the homotopy analysis method, Sajid and Hayat [2] investigated the effect of thermal radiation on the boundary layer flow caused

by an exponentially stretched sheet. MHD research has a wide range of applications, including the cooling of nuclear reactors with liquid sodium and the induction flow meter, which is based on the potential difference in the fluid in the direction perpendicular to the motion and the magnetic field. The electric conductivity of nano fluid in a vertical permeable circular cylinder is investigated [3]. Copper and silver nanoparticles are utilised in place of regular liquid ethylene glycol.The relationship between particle form and radiation impacts on Marangoni boundary layer flow and heat transfer of Cu, Al2O3, and SWCNTs based on water, ethylene glycol, and engine oil[4]. Melting heat transportation in radiative flow of nanomaterials with irreversibility analysis and heat transportation in electro-magnetohydrodynamic flow of Darcy-Forchheimer viscous fluid with irreversibility analysis. [5, 6, 7] Oyelakin et al. [8] explains Increases in the Casson, Dufour, and unsteadiness indices diminish fluid velocity, temperature, and concentration profiles, according to the study. Raising thermal radiation raises temperature profiles, and increasing the Soret parameter raises concentration profiles, as expected. For vertical and horizontal heaters in the cavity, heat transfer is dug out. The base fluid ethylene glycol is investigated in conjunction with Ag nanoparticles. When a horizontal heater is put in the centre of the cavity, heat transfer in the enclosure filled with nanofluid is improved in the case of Cattaneo–Christov heat flux [9]. The flow and heat transmission of water and ethylene glycol-based copper nanoparticles between two parallel squeezing discs with suction/injection effects are investigated by Rizwan-ul-Haq et al. [10] They found magnetic fields have a large influence on metallic particles, evaluated the MHD effect, which is normal to the surface, and the lower disc is considered permeable. Saqib et al. [11] investigate the flow of an isothermal vertical plate with an ethylene glycol-based molybdenum disulfide generalized nanofluid. The spherical molybdenum disulfide nanoparticles are suspended in ethylene glycol, a common base fluid. Entropy analysis for magnetohydrodynamic (MHD) unsteady flow of Prandtl fluid by a stretchable surface is addressed. Thermal transport with radiation, magnetic field and dissipation is taken. Physical behaviors of Soret and Dufour impacts are examined by Khan et al. [12]. Nadeem et al. [13] investigated two-dimensional boundary layer flow and heat transmission in a steady incompressible OldroydB nanofluid. They discovered that as the Brownian motion parameter was raised, the local Nusselt number decreased while the local Sherwood number rose. Makinde et al.[14]investigated the combined effects of buoyancy force, convective heating, Brownian motion, thermophoresis, and a magnetic field on stagnation point flow and heat transfer due to a nanofluid flow from a stretching/shrinking sheet. Their findings revealed that for the shrinking case, dual solutions exist, and that increasing the buoyancy force reduced both the skin friction coefficient and the local Sherwood number while increasing the local Nusselt number. Haroun et al. [15] investigated heat and mass transport in a magnetohydrodynamic mixed convection flow of a nanofluid over an unsteady stretching/shrinking sheet in a magnetohydrodynamic mixed convection flow of a nanofluid. The flow was subjected to a heat source as well as viscous dissipation. The effects of Soret and Dufour were expected to be significant. In hydromagnetic flows, viscous dissipation behaves like a volumetric heat source, while Joule dissipation behaves like a viscous heat source. In the heat treated materials contained among the nourished and wind-up rolls, the combined Joule and viscous dissipations influence is very sig-

nificant [16, 17, 18]. Rao et al. [19]examined the impacts of chemical reaction, thermal radiation, magnetic, suction, porosity, and joule heating factors in a numerical analysis corresponding to the flow and heat transfer in a steady flow region of nanofluid across an exponential stretching surface. Elbashbeshy [20] looked at how suction affected laminar flow across an increasingly stretched surface. El-Aziz[21] investigated the mixed convective flow of a micro-rotating fluid propelled by a stretched surface. Aziz and Khan [22] explored the natural convection flow of nanofluid through convective boundary conditions. Silver, Copper, Copper oxide, Titanium oxide, and Aluminum oxide are among the nanoparticles investigated by Ahmad and Mustafa [23]. Thermal conductivity performance for ternary hybrid nanomaterial subject to entropy generation is describe and Simultaneous features of soret and dufour in entropy optimized flow of reiner-rivlin fluid considering thermal radiation by Khan et al. [24, 25, 26]. In the present article, the importance of the ethylene glycol-based C_u nanoparticle through a exponential stretching sheet with several parameters, such as Dufour,thermal radiation, MHD, Eckart number were tested for their effects on fluid flow, heat and mass transfer profiles, and thermal convective boundary conditions with simultaneous impact of Navier velocity slip. Nanofluid framework has been updated to include thermophoresis and Brownian motion. Because of their small size, nanoparticles have a high surface to volume ratio. In the field, surface cooling and heating are widespread. It is impossible to hide the presence of convective heat exchange between the surface and the surrounding fluid. The governing partial differential equations are reduced using the similarity transformation, then converted to a set of non-linear ordinary differential equations that are numerically solved using Matlab's bvp4c method. The impacts of numerous physical parameters on dimensionless velocities, concentration, temperature profiles, skin friction, and Nusselt number were demonstrated using tables and graphs.

2. Physical Model and Mathematical Formulation

A steady, two-dimensional, incompressible flow of ethylene glycol-based C_u nanofluid has been explored as it passes over an exponentially stretching sheet. Figure 1 shows the x-axis running along the stretched sheet in the flow direction and the y-axis running parallel to the flow direction. Furthermore, the magnetic field B_o is applied to the fluid flow in a normal direction. In the energy equation, the effects of Joule heating and thermal radiation phenomena are investigated further. The sheet is stretched with the linear velocity $U_w = exp(\frac{x}{l})$ and is regarded a heated fluid with the$-k_{nf}\frac{\partial T}{\partial y} = h_f(T_f - T)$ wall. The basic continuity, momentum, energy equation,and concentration equations for this situation can be expressed as follows using the foregoing assumptions and the model equations presented by Tiwari and Das [27, 28, 29]

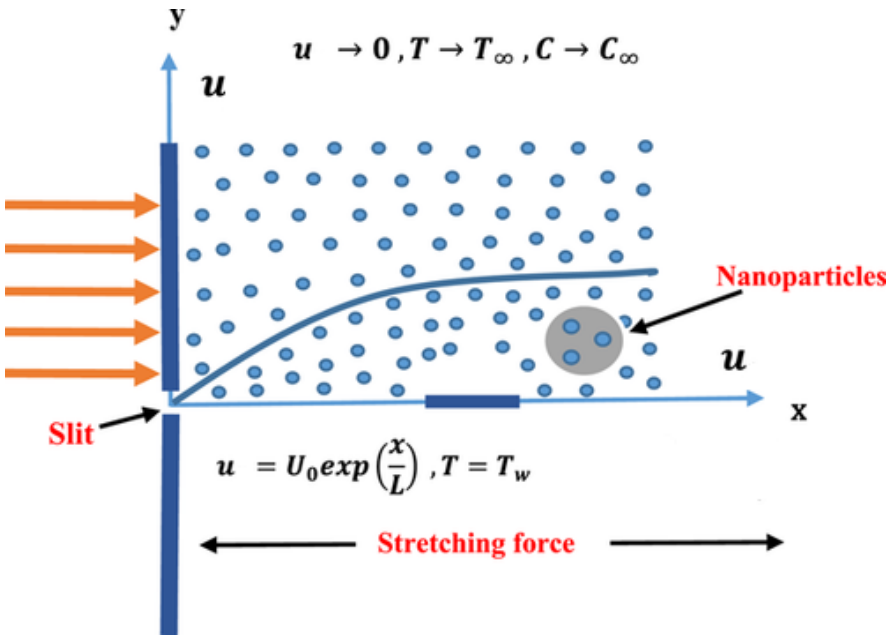

Figure 1: Physical flow diagram

In vector form:

$$\nabla . V = 0 \tag{1}$$

$$(V.\nabla)\, V = \frac{1}{\rho_{nf}} \left(\nabla(\mu \nabla V) + \sigma_{nf}(B_o * j)\right) \tag{2}$$

$$(V.\nabla)\, T = \frac{1}{(C_p \rho)_{nf}} \left(\nabla(\kappa_{nf} \nabla T) + \frac{1}{\sigma_{nf}}(j.j) + \tau(D_B(\nabla .T.\nabla C) + \frac{D_T}{D_\infty}(\nabla T.\nabla T)) - \nabla .q_r\right) \tag{3}$$

$$(V.\nabla)\, C = \nabla . \left(D(\nabla C) + \frac{D_T}{D_\infty}(\nabla T)\right) \tag{4}$$

V denotes the velocity vector which has the components V(u(x,y), v(x,y)). j denotes the electric current density which is formulated by generalized Ohm's law including Hall current as [30]

$$\frac{\partial u}{\partial x} + \frac{\partial v}{\partial y} = 0 \tag{5}$$

$$u\frac{\partial u}{\partial x} + v\frac{\partial v}{\partial y} = \nu_{nf}\frac{\partial^2 u}{\partial y^2} - \frac{\sigma_{nf}(B_o)^2}{\rho_{nf}} u \tag{6}$$

$$u\frac{\partial T}{\partial x} + v\frac{\partial T}{\partial y} = \frac{\kappa_{nf}}{(\rho c_p)_{nf}}\frac{\partial^2 T}{\partial y^2} - \frac{1}{(\rho c_p)_{nf}}\frac{\partial q_r}{\partial y} + \tau\left[D_B\left(\frac{\partial T}{\partial y}\frac{\partial C}{\partial y}\right) + \frac{D_T}{T_\infty}\left(\frac{\partial T}{\partial y}\right)^2\right] + \frac{\sigma_{nf}(B_o)^2 u^2}{(\rho c_p)_{nf}} \tag{7}$$

$$u\frac{\partial C}{\partial x} + v\frac{\partial C}{\partial y} = \frac{\partial^2 C}{\partial y^2} + \frac{D_T}{T_\infty}(\frac{\partial^2 T}{\partial y^2}) \tag{8}$$

In addition, (u, v) represents the velocity component in the x and y directions, respectively, and T represents the fluid temperature. Furthermore,τ is the ratio of the nanoparticle material's heat capacity to the fluid's heat capacity.

Brownian diffusion coefficient and thermophoretic diffusion coefficient, are represented by D_B,D_T respectively. The above problem's boundary conditions are as follows:

$$u = U + N\nu_f \frac{\partial U}{\partial y}, v = 0, -k_{nf}\frac{\partial T}{\partial y} = h_f(T_f - T), C_w \ \ at \ \ y = 0$$
$$u \longrightarrow 0, T \longrightarrow T_\infty, C \longrightarrow C_\infty \ \ at \ \ y \longrightarrow \infty \tag{9}$$

where T_f denotes the temperature at the wall and T_∞ denotes the ambient temperature Also N, B_o,μ_{nf}, ρ_{nf}, h_f are the slip velocity factor, magnetic field parameter, dynamic viscosity, the density of the based fluid and the convective heat transfer coefficient respectively. The Rosseland [31] approximation is expressed in terms of radiative heat flux as follows:

$$q_r = \frac{4\ \alpha^* \partial^4 T}{3\ K_1 \partial y^2}$$

where K_1 is the Roseland mean absorption coefficient and α^* is the Stefan Boltzman constant. When minimal temperature variations in the flow are explored, Taylor series is used after ignore the higher-order term [32], we get

$$q_r = \frac{4\ \alpha^*}{3\ K_1}\frac{\partial^4 T}{\partial y^4} = \frac{16\ \alpha^* T_\infty^3}{3\ K_1}\frac{\partial T}{\partial y} \tag{10}$$

The consistent characteristics are retained with the exception of density changes that create a thermal buoyancy force. The thermophysical properties of C_u and ethylene glycol are showcased in Table1 and these values are extracted from[33, 34].

Table 1: Properties of particle and base fluid

Physical properties	$\rho(kg.m^{-3})$	$C_p(J(kg.K)^{-1})$	$\kappa(W(K.m)^{-}1)$	$\beta(K^{-1})$
$Ethylene\ Gylcol$	1114.4	2415	0.252	$57 * 10^{-5}$
C_u	8933	385	401	$1.67 * 10^{-5}$

The effective nanofluid properties [35, 36, 37] are given by

$$\rho_{nf} = \phi\frac{(\rho c_p)_s}{(\rho c_p)_f} + (\rho c_p)_f(1-\phi), \qquad (\rho c_p)_{nf} = \phi\rho_s + \rho_f(1-\phi)$$
$$\frac{\kappa_{nf}}{\kappa_f} = \frac{2\kappa_f + \kappa_s - 2\phi(\kappa_f - \kappa_s)}{2\kappa_f + \kappa_s + \phi(\kappa_f - \kappa_s)}, \quad \frac{\mu_{nf}}{\mu_f} = \frac{1}{(1-\phi)^{2.5}} \tag{11}$$

Where $\mu_f$is the dynamic viscosity of the base fluid,ϕ is the solid volume fraction ρ_f and ρ_s are the densities, κ_f and κ_s are the thermal conductivities , σ is the electrically conductivities,$(\rho c_p)_f$ and $(\rho c_p)_s$ are the heat capacitance of the base fluid and nanoparticles, respectively. The following similarity transforms are used to convert the equations (2) to

(4) to ordinary differential equations [38].

$$u = U_o e^{\frac{X}{L}} f'(\eta),\ \theta(T_f - T_\infty) = (T - T_\infty),\ \eta = y\sqrt{\frac{U_o}{2L\nu_f}} e^{\frac{2X}{L}},$$
$$\psi(C_f - C_\infty) = (C - C_\infty),\ \ v = y\sqrt{\frac{U_o \nu_f}{2L}} e^{\frac{2X}{L}} (f(\eta) + \eta f'(\eta)) \tag{12}$$

The dimensionless coordinate is represented by η.

$$\frac{A_1}{A_2}\frac{\partial^3 f}{\partial \eta^3} - \frac{\partial f}{\partial \eta}^2 + f\frac{\partial^2 f}{\partial \eta^2} - \frac{M}{A_2}\frac{\partial f}{\partial \eta} = 0 \tag{13}$$
$$\frac{1}{A_3 P_r}(A_4 + Rd)\frac{\partial^2 \theta}{\partial \eta^2} + \frac{M E_c}{A_3}(\frac{\partial f}{\partial \eta})^2 + N_B \frac{\partial \theta}{\partial \eta}\frac{\partial \psi}{\partial \eta} + N_t(\frac{\partial \theta}{\partial \eta})^2 + f\frac{\partial \theta}{\partial \eta} = 0 \tag{14}$$
$$\frac{\partial^2 \psi}{\partial \eta^2} - S_c f\frac{\partial \psi}{\partial \eta} - \frac{N_t}{N_B}\frac{\partial^2 \theta}{\partial \eta^2} = 0 \tag{15}$$

with boundary conditions

$$f(\eta) = 0, \quad \frac{\partial f}{\partial \eta} = 1 + \lambda\frac{\partial^2 \theta}{\partial \eta^2}, \quad A_4\frac{\partial \theta}{\partial \eta} - Bi\theta(\eta) = -Bi, \psi = 1 \ \ at \ \ \eta = 0$$
$$\frac{\partial f}{\partial \eta} \longrightarrow 0, \quad \beta \longrightarrow 0, \quad \theta(\eta) \longrightarrow 0, \psi(\eta) \longrightarrow 0, \ \ at \ \ \eta \longrightarrow \infty \tag{16}$$

Here,

$$A_1 = \frac{\mu_{nf}}{\mu_f} = \frac{1}{(1-\phi)^{2.5}}, \quad A_3 = \phi\frac{(\rho c_p)_s}{(\rho c_p)_f} + (\rho c_p)_f(1-\phi)$$
$$A_4 = \frac{2\kappa_f + \kappa_s - 2\phi(\kappa_f - \kappa_s)}{2\kappa_f + \kappa_s + \phi(\kappa_f - \kappa_s)}, \qquad A_2 = \phi\rho_s + \rho_f(1-\phi) \tag{17}$$

The effective thermal conductivity of fluid can be determined by Maxwell–Garnett's (MG model) self-consistent approximation model, effective density, specific heat and thermal conductivity of nanofluid by Tiwari and Das[35] the magnetic field parameter M,Prandtl number P_r, number N_B, N_t, Biot number B_i, and thermophoretic variable N_t, Schmidt number S_c, Eckert number E_c, Brownian diffusion N_B, slip effect λ and radiation parameter R_d .

$$M = \frac{\sigma_f {B_O}^2}{\rho_f a}, \quad E_c = \frac{{U_m}^2}{(T_f - T_\infty)(C_p)_f}, \quad P_r = \frac{(\mu c_p)_f}{\kappa_f}, \quad S_c = \frac{(\nu_f}{D_B}$$
$$R_d = \frac{16\alpha^* T^3}{3K_1\kappa_f}, \quad N_B = \frac{\tau D_B(C_w - C_\infty)}{\nu_f}, N_t = \frac{\tau D_t(T_w - T_\infty)}{\nu_f T_\infty}, \quad \lambda = N_o\sqrt{\frac{(U_o\nu_f)}{2L}}, \quad B_i = \frac{h_f}{\kappa_f}\sqrt{\frac{\nu_f}{a}}. \tag{18}$$

3. Engineering Quantities

Skin friction coefficient Cf_x and Nusselt number Nu_x are defined as

$$Cf_x = \frac{\tau_w}{u_w \rho_f}\frac{\partial u}{\partial y}, \quad Nu_x = \frac{x q_w}{\kappa_f \left(T_f - T_\infty\right)}, \quad Sh_x = \frac{x q_m}{D_m \left(C_f - C_\infty\right)} \tag{19}$$

where $q_w,\ \tau_w\ q_m$ are heat flux,shear stress,designates the mass flux from the surface respectively. The dimensionless local skin friction coefficient Cf_x and Nusselt number Nu_x and the local Sherwood number Sh_x are

$$\frac{1}{2}\sqrt{Re_x}Cf_x = \frac{\partial^2 f(0)}{\partial \eta^2}, \quad \frac{Nu_x}{\sqrt{Re_x}} = -(A_4 + R_d)\frac{\partial \theta(0)}{\partial \eta}, \quad \frac{Sh_x}{\sqrt{Re_x}} = -\frac{\partial \psi(0)}{\partial \eta} \tag{20}$$

where $\sqrt{Re_x} = \frac{\sqrt{a}x}{\sqrt{\nu_f}}$ is Reynold number.

4. Method of Solution and Validation

Equations along with the boundary conditions are resolved numerically by bvp4c solver, a MATLAB built-in function.The solver of bvp4c is a finite difference code that uses the three-stage Lobatto IIIa implicit Runge–Kutta formula which gives the numerical solution of fourth-order. The solutions are derived from an initial guess. It is necessary to choose the appropriate initial guess and the thickness of the boundary layer based on the values of the parameters[39, 40]. Now, first reduce the equations to a system of first-order ordinary differential equations. Thus the set of equations(13-15) is stated as,

$$f = y_1, \ \ f' = y_2, \ \ f'' = y_3 \tag{21}$$

$$f''' = A_1\left[A_2(2(y_2)^2 - y_1 y_3) + M y_2\right] \tag{22}$$

$$\theta = y_4, \ \ \theta' = y_5, \ \ \theta'' = \frac{-P_r}{[A_4 + R_d]}\left[M{E_c}{y_2}^2 + A_3(N_B y_7 y_5 + N_t(y_5)^2 + y_1 y_5\right] \tag{23}$$

$$\psi = y_6, \ \ \psi' = y_7, \ \ \psi'' = -\left[S_c y_7 y_1 + \frac{N_t}{N_B}\frac{-P_r}{[A_4 + R_d]}\left[M{E_c}{y_2}^2 + A_3(N_B y_7 y_5 + N_t(y_5)^2 + y_1 y_5\right]\right] \tag{24}$$

Now boundary conditions as

$$y_1^a = 0, \ \ y_2^a = 1 + \lambda y_3, \ \ A_4 y_5^a - B_i y_4^a + B_i = 0, y_6^a = 1$$
$$y_2^r = 0, \ \ y_4^r = 0, \ \ y_6^r = 0 \tag{25}$$

The solver's syntax soll = bvp4c(@OdeBVP, @OdeBC, solinit) @OdeBVP, into which the equation (22-24) are coded. Then, the boundary conditions(25) are coded into the function handle @OdeBC. The mesh points and initial approximation of the solution are coded using solinit the points of the initial mesh and initial approximation of the solution

at the mesh points are coded in solinit [41]. One must guess the desired solution for the ordinary differential equation. As long as the guess is accurate, it should satisfy boundary conditions and reveal the behavior of the solution. A preliminary guess of the solution is not difficult, since the bvp4c method can converge to it even if the initial guess is poor. We use the obtained results as an initial guess for the solution of the problem with only a small variation of the parameters. In this way, we repeatedly adjust the parameters until they are as close as possible to the right values. This method is described in the book by Shampine et al.[42]. Through a comparison of the current work with previously published works, the current problem has been validated and the code has been verified as accurate. A commendable agreement is noted table 2 at $\eta = 40$.

Table 2: Comparison of $-\theta'(0)$ for different values of P_r while all the other parameters are fixed

P_r	Magyari and Keller [43]	D.Srinivasacharya1 and P.Jagadeeshwar1 [44]	Present result
0.5	0.330493	0.330537	0.330493
1.0	0.549643	0.549643	0.549643
3.0	1.122188	1.122086	1.122089
5.0	1.521243	1.521238	1.521239
8.0	1.991847	1.991836	1.9918390
10.0	2.257429	2.257422	2.2574254

5. Concluding Results

The consequences of various influential parameters on velocity $f^{'}(\xi)$, concentration $(\psi(\xi))$, and temperature $(\theta(\xi))$ profiles are illustrated in Figures with magnetic field parameter $M = 0.01$, Prandtl number $P_r = 150.45$, thermophoretic variable $N_t = 0.1$, Biot number $B_i = 0.1$, Schmidt number $S_c = 0.4$, Eckert number $E_c = 0.3$, Brownian diffusion $N_B = 0.3$,slip effect $\lambda = 0.5$ and radiation parameter $R_d = 0.5$ respectively are taken otherwise mentioned.

Figure 2(a-b), depicting as M rises, the velocity profile reduces, while the temperature profile increases in the presence and absence of slip effect λ. Simultaneous effect of slip and magnetic parameters. Remarkably, a greater magnetic force inhibits nanofluid flow. The width of the momentum boundary layer decreased as the velocity profile decreased, whereas as M increased, the Lorentz force in the magnetic field increased. The magnetic field creates an opposing/resistive force known as the Lorentz force, which reduces fluid velocity and thins the flow boundary layer.

Figure 3(a) illustrates fluid temperature rises as the Eckert number E_c and slip parameter rises. The increased dissipative heat induced by higher viscosity causes a fluid's temperature to rise. The presence of Eckert number in nanofluid increases the intensity of thermal energy production, resulting in better temperature distributions and hence thicker thermal layers. The energy caused by frictional heat from the flow is converted into internal energy inside the fluid, which is then stored. Also the inverse relationship between surface slipperiness and fluid temperature, means raising the slip parameter tends to raise fluid temperature. As the temperature rises, the thickness of the thermal

Table 3: The variation of the Nusselt number (Nu_x), skin friction coefficient (Cf_x) and Sherwood number for different values of M, R_d, W, λ while other parameters remain fixed

M	λ	R_d	B_i	$Nu_x Re_x^{-1/2}$	$-\frac{1}{2}C_f x_x^{-1/2}$	$Sh_x Re_x^{-1/2}$
0	0.2	0.5	0.2	0.281470	0.979396	-0.038852
0.1	-	-	-	0.271511	1.001847	-0.034269
0.5	-	-	-	0.235195	1.083861	-0.017071
0.7	-	-	-	0.218747	1.121052	-0.009132
0.2	0.2	0.5	0.2	0.261939	1.023443	-0.029795
-	0.4	-	-	0.264232	0.810002	-0.043344
-	0.7	-	-	0.266164	0.623996	-0.056729
-	1.0	-	-	0.267249	0.510861	-0.065875
0.2	0.2	0.1	0.2	0.195584	1.023443	-0.028931
-	-	0.3	-	0.228775	1.023443	-0.029435
-	-	0.5	-	0.261939	1.023443	-0.029795
-	-	0.7	-	0.2950721	1.023443	-0.030055
0.2	0.2	0.5	0.05	0.067253	1.023443	0.089807
-	-	-	0.1	0.133310	1.023443	0.049222
-	-	-	0.3	0.386078	1.023443	-0.106043
-	-	-	0.5	0.621619	1.023443	-0.250682

boundary layer increases. As a result, we can deduce that the rate of heat transmission reduces as the slip parameter increases. The temperature distribution broadened as the thermal radiation parameter R is raised is shown in figure 3(b). Physically when radiation parameter R_d is increased, the fluid discharges heat energy from the flow area, boosting the temperature of the nanofluid and cooling the system. A high value for the radiation parameter contributes more heat to the system, and the thickness of the thermal boundary layer. The thermal field increases as κ increases because the mean absorption coefficient decreases. As a result, heat radiation should be kept to a bare minimum for a more efficient cooling process.

According to the figure 4(a), Brownian diffusion N_B on a temperature field with simultaneously effect of slip parameter. Brownian motion is the disordered movement of suspended particles in a liquid produced by collisions. The unsystematic movement of suspended nanoparticles increases as the system's internal energy rises, and the thermal field rises as a result for greater values of Brownian diffusion. Figure 4(b) explain the behaviour of N_B with concentration layer. As Brownian diffusion magnitude grows, the stride during which nanoparticles move in a random path subject to varied velocities increases. As a result, higher N_B equals lesser concentration layer and vice versa.

Figure 5(a-b) presentation is to show how boost the thermophoretic variable N_t disrupts the temperature and concentration field. The both field appears to be higher here due to the larger thermophoretic variable. Physically the thermophoretic parameter boost the convection process in the current flow analysis, causing material elements to migrate from a heated to a cold surface. Kinetic energy is created when elements are transferred from one surface to another, and the temperature field rises as a result. The simultaneous impact of Schmidt number S_c and velocity slip λ parameters on the thermal layer and concentration field depicting in figures 6(a) and 6 (b). The temperature profile

Table 4: The variation of the Nusselt number (Nu_x), and Sherwood number for different values of N_t, N_B, E_c, while other parameters remain fixed

E_c	N_t	N_B	$Nu_x Re_x^{-1/2}$	$Sh_x Re_x^{-1/2}$
0.1	0.2	0.3	0.269495	0.017084
0.3	-	-	0.247896	0.030569
0.5	-	-	0.225844	0.044336
0.2	0.2	0.3	0.258750	0.023793
-	0.3	-	0.258424	-0.026446
-	0.5	-	0.257734	-0.126245
-	0.7	-	0.256986	-0.225046
0.2	0.2	0.1	0.264615	-0.189596
-	-	0.4	0.254912	0.050892
-	-	0.6	0.244483	0.078847
-	-	0.7	0.237306	0.087354

increases with increase in whereas opposite behaviour show in concentration profile. The concentration field reduced with grow in S_c. The physical significance of Schmidt's number As the Schmidt number rises, the momentum diffusivity rises with it. It dilutes the fluid's molecular diffusivity, which decreases the concentration boundary layer. As a result, the liquid concentration decreases. In figure 7(a) it is observed that when slip parameter λ increases, the velocity component near the wall decreases, eventually reaching zero at the boundary layer's edges. Therefore, as the slip parameter increases, the hydrodynamic boundary layer thickness decreases and the local velocity decreases. This measure corresponds to the idea that a higher score means there is more lubrication and slipperiness on the surface. The slip at the surface wall increases as the slip parameter increases, resulting in a lower fluid penetration. When slip is absent,$f(0) = 1$ and approaches zero. With increasing Biot number B_i, the thermal boundary layer is observed to be a significantly growing feature of fluid layers show in figure 7(b). In principle, a larger B_i corresponds to more convective heating at the sheet, which raises the temperature gradient. When the temperature differential is greater, the thermal influence can permeate deeper into the quiescent fluid. Furthermore, as the Biot number on the right side of the stretching sheet grows, the fluid temperature increases, lowering the sheet's thermal resistance and increasing convective heat transfer

Table3-4 elucidate the variation of pertinent parameters on heat transfer, drag coefficient and mass transfer. Further a decreasing effects on the local nusselt number with increasing in E_c,N_B and magnetic field M local Sherwood number increased with these parameters whereas it both physical quantities show same effect with rise in N_t. While nusselt number reinforce with increasing in parameters λ,radiationR_d, Biot number B_i. Also local skin friction coefficient and velocity profiles decreases with increasing in slip parameters λ.

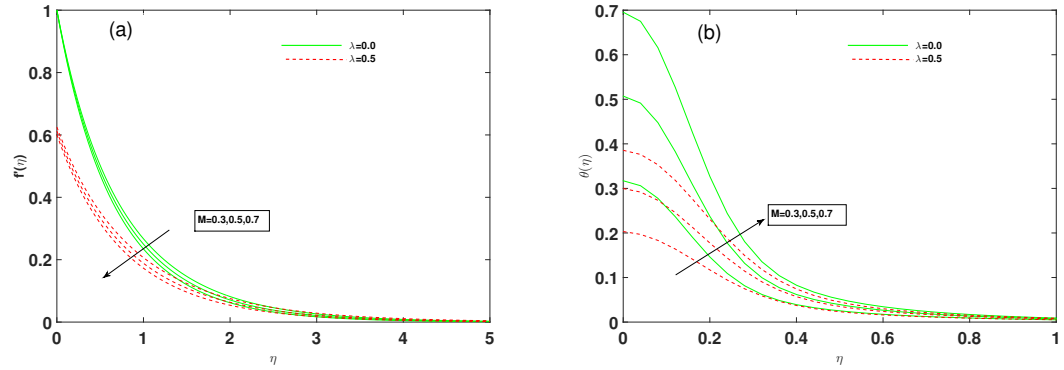

Figure 2: Variation in velocity And temperature profile with different values of M and λ

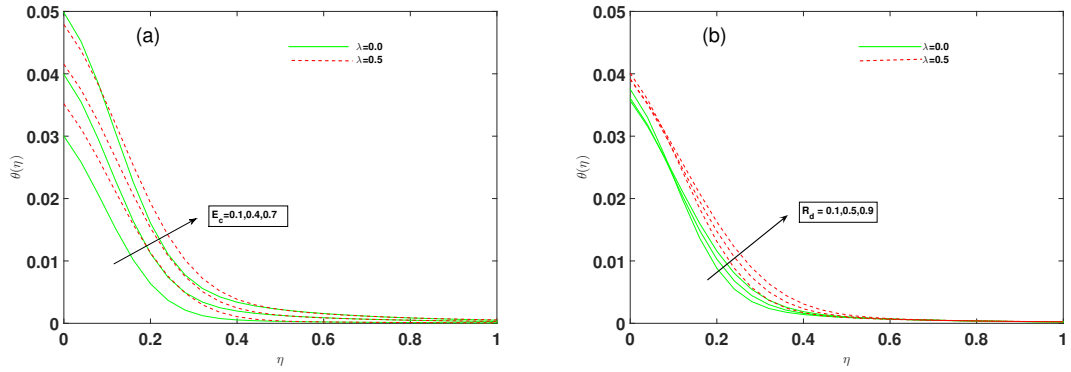

Figure 3: Variation in temperature profile with E_c and R_d at different values of λ

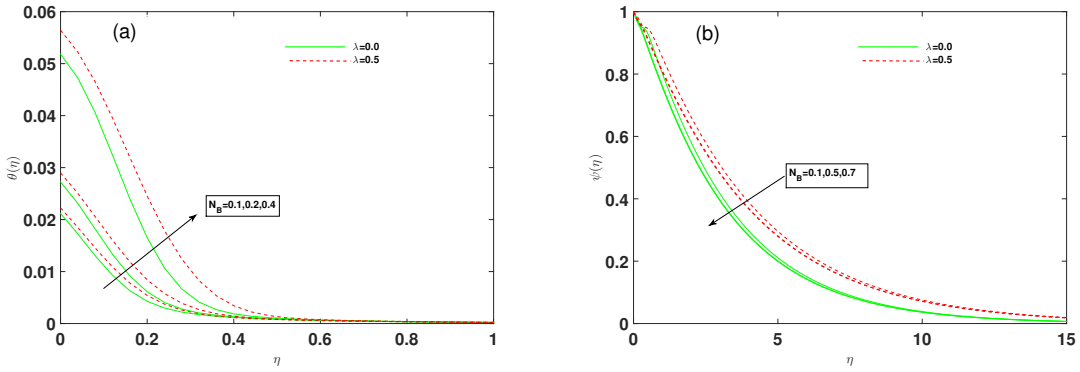

Figure 4: Variation in temperature and concentration profile with N_B at different values of λ

6. Conclusions

This study used an exponential stretching sheet with numerous parameters like Dufour, thermal radiation, MHD, and Eckart number to observe how they affected fluid flow, heat and mass transfer profiles, and thermal convective boundary conditions with the simultaneous effect of Navier velocity slip. The governing partial differential equations

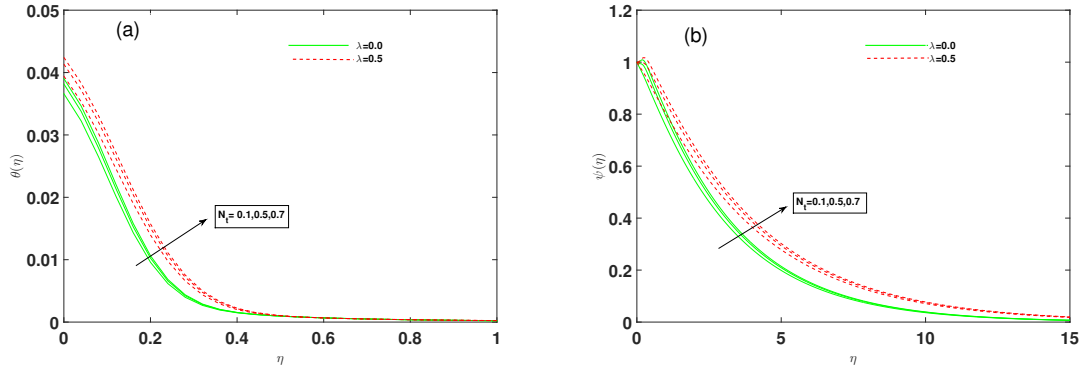

Figure 5: Variation in temperature and concentration profile with N_t at different values of λ

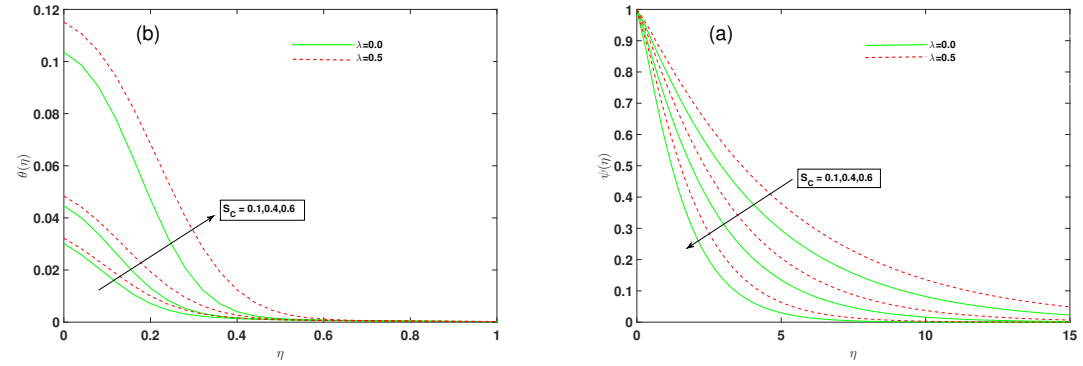

Figure 6: Variation in temperature and concentration profile with N_B at different values of λ

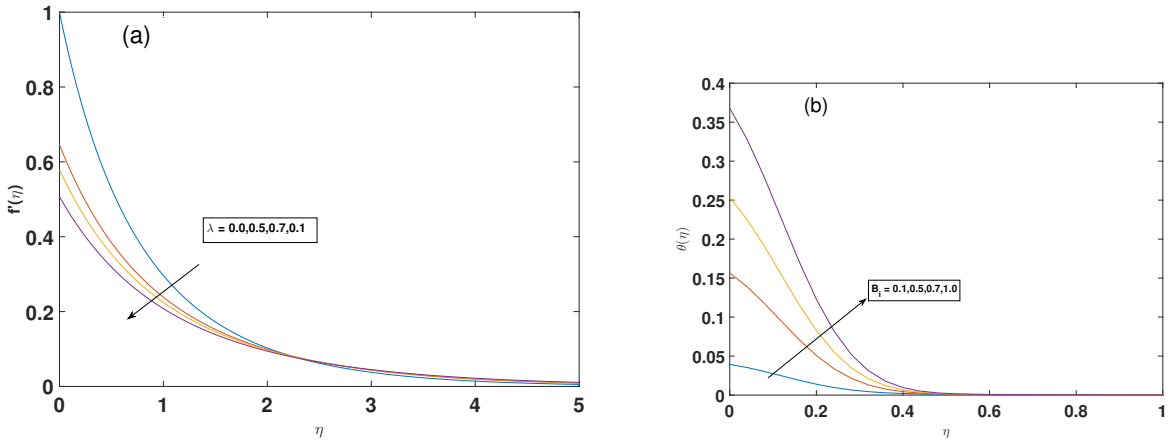

Figure 7: Fluctuation of velocity and temperature profiles along with variation of parameters λ and B_i respectively

are simplified using the similarity transformation and then converted ordinary differential equations are solved using Matlab's bvp4c approach. Due to the complicated nature of the variables impacted by the controlling factors, the following results are noteworthy:

- The concentration of nanoparticles is observed to be a declining function of both the Schmidt number S_c and Brownian motion N_B, although the concentration increases when thermophoretic variable N_t rises.
- The velocity and momentum boundary layer thickness are reduced for larger values of λ and magnetic field M.
- The Nusselt number are the decreasing functions of parameter magnetic field M, Eckert number E_c and N_B but the local Sherwood numbershow opposite behavior with these parameters.
- The velocity profile and local skin friction of nanofluid is reduced due to increasing slip parameter.
- The impact of the thermal radiation parameter, magnetic parameter, and Biot number is magnified, the irreversibility of thermal energy increases. The Nusselt number intensifies with radiation parameter R_d, λ and Biot numberB_i.

Table 5: Nomenclature

quantity	Symbol	Unit
Ambient fluid temperature	T_∞	K
fluid temperature	T	K
Length of sheet	L	m
Far field velocity	U	ms^{-1}
Thermal conductivity	k_{nf}	$WK^{-1}m^{-1}$
Specific heat capacity	C_p	$Jg^{-1}K^{-1}$
Density	ρ_{nf}	$m^{-3}kg^{1}$
Viscosity	μ_{nf}	$Nm^{-2}s^{1}$
Boltzmann's constant	κ	JK^{-1}
Kinematic Viscosity	ν_{nf}	m^2s^{-1}
Electrical conductivity	σ	$A^2kg^{-1}m^{-3}s^3$

References

References

[1] S. U. Choi, J. A. Eastman, Enhancing thermal conductivity of fluids with nanoparticles, Tech. rep., Argonne National Lab.(ANL), Argonne, IL (United States) (1995).

[2] M. Sajid, T. Hayat, Influence of thermal radiation on the boundary layer flow due to an exponentially stretching sheet, International Communications in Heat and Mass Transfer 35 (3) (2008) 347–356.

[3] M. Gholinia, S. Gholinia, K. Hosseinzadeh, D. Ganji, Investigation on ethylene glycol nano fluid flow over a vertical permeable circular cylinder under effect of magnetic field, Results in Physics 9 (2018) 1525–1533.

[4] N. A. Adnan, R. Kandasamy, R. Mohammad, Nanoparticle shape and thermal radiation on marangoni water, ethylene glycol and engine oil based cu, al2o3 and swcnts, Journal of Material Sciences & Engineering 6 (4) (2017).

[5] S. A. Khan, T. Hayat, A. Alsaedi, B. Ahmad, Melting heat transportation in radiative flow of nanomaterials with irreversibility analysis, Renewable and Sustainable Energy Reviews 140 (2021) 110739.

[6] M. I. Khan, S. A. Khan, T. Hayat, M. Waqas, A. Alsaedi, Modeling and numerical simulation for flow of hybrid nanofluid (sio2/c3h8o2) and (mos2/c3h8o2) with entropy optimization and variable viscosity, International Journal of Numerical Methods for Heat & Fluid Flow (2019).

[7] T. Hayat, S. A. Khan, A. Alsaedi, H. M. Fardoun, Heat transportation in electro-magnetohydrodynamic flow of darcy-forchheimer viscous fluid with irreversibility analysis, Physica Scripta 95 (10) (2020) 105214.

[8] I. S. Oyelakin, S. Mondal, P. Sibanda, Unsteady casson nanofluid flow over a stretching sheet with thermal radiation, convective and slip boundary conditions, Alexandria engineering journal 55 (2) (2016) 1025–1035.

[9] N. Muhammad, S. Nadeem, A. Issakhov, Finite volume method for mixed convection flow of ag–ethylene glycol nanofluid flow in a cavity having thin central heater, Physica A: Statistical Mechanics and its Applications 537 (2020) 122738.

[10] Z. Khan, S. Hussain, Z. Hammouch, et al., Flow and heat transfer analysis of water and ethylene glycol based cu nanoparticles between two parallel disks with suction/injection effects, Journal of Molecular Liquids 221 (2016) 298–304.

[11] M. Saqib, F. Ali, I. Khan, N. A. Sheikh, S. B. Shafie, Convection in ethylene glycol-based molybdenum disulfide nanofluid, Journal of Thermal Analysis and Calorimetry 135 (1) (2019) 523–532.

[12] S. A. Khan, T. Hayat, A. Alsaedi, Numerical study for entropy optimized radiative unsteady flow of prandtl liquid, Fuel 319 (2022) 123601.

[13] S. Nadeem, R. Ul Haq, N. S. Akbar, C. Lee, Z. H. Khan, Numerical study of boundary layer flow and heat transfer of oldroyd-b nanofluid towards a stretching sheet, PloS one 8 (8) (2013) e69811.

[14] O. Makinde, W. Khan, Z. Khan, Buoyancy effects on mhd stagnation point flow and heat transfer of a nanofluid past a convectively heated stretching/shrinking sheet, International Journal of Heat and Mass Transfer 62 (2013) 526–533.

[15] N. A. Haroun, P. Sibanda, S. Mondal, S. S. Motsa, On unsteady mhd mixed convection in a nanofluid due to a stretching/shrinking surface with suction/injection using the spectral relaxation method, Boundary value problems 2015 (1) (2015) 1–17.

[16] G. Seth, J. Singh, Mixed convection hydromagnetic flow in a rotating channel with hall and wall conductance effects, Applied Mathematical Modelling 40 (4) (2016) 2783–2803.

[17] G. Seth, S. Sarkar, O. Makinde, Combined free and forced convection couette-hartmann flow in a rotating channel with arbitrary conducting walls and hall effects, Journal of Mechanics 32 (5) (2016) 613–629.

[18] G. S. Seth, R. Sharma, M. K. Mishra, A. J. Chamkha, Analysis of hydromagnetic natural convection radiative flow of a viscoelastic nanofluid over a stretching sheet with soret and dufour effects, Engineering Computations (2017).

[19] J. A. Rao, G. Vasumathi, J. Mounica, et al., Joule heating and thermal radiation effects on mhd boundary layer flow of a nanofluid over an exponentially stretching sheet in a porous medium, World Journal of Mechanics 5 (09) (2015) 151.

[20] E. Elbashbeshy, Heat transfer over an exponentially stretching continuous surface with suction, Archives of Mechanics 53 (6) (2001) 643–651.

[21] M. Abd El-Aziz, Viscous dissipation effect on mixed convection flow of a micropolar fluid over an exponentially stretching sheet, Canadian Journal of Physics 87 (4) (2009) 359–368.

[22] A. Aziz, W. Khan, Natural convective boundary layer flow of a nanofluid past a convectively heated vertical plate, International Journal of Thermal Sciences 52 (2012) 83–90.

[23] R. Ahmad, M. Mustafa, Model and comparative study for rotating flow of nanofluids due to convectively heated exponentially stretching sheet, Journal of Molecular Liquids 220 (2016) 635–641.

[24]

[25] S. A. Khan, T. Hayat, A. Alsaedi, Simultaneous features of soret and dufour in entropy optimized flow of reiner-rivlin fluid considering thermal radiation, International Communications in Heat and Mass Transfer 137 (2022) 106297.

[26] S. A. Khan, T. Hayat, A. Alsaedi, Entropy optimization for nanofluid flow with radiation subject to a porous medium, Journal of Petroleum Science and Engineering 217 (2022) 110864.

[27] B. Nayak, S. Mishra, R. Tripathy, Interaction of cu and ag nanoparticles on mhd water-based nanofluids past a stretching sheet, Heat Transfer—Asian Research 48 (8) (2019) 3425–3445.

[28] P. Loganathan, C. Vimala, Mhd boundary layer flow of a nanofluid over an exponentially stretching sheet in the presence of radiation, Heat Transfer—Asian Research 43 (4) (2014) 321–331.

[29] P. Kameswaran, M. Narayana, P. Sibanda, G. Makanda, On radiation effects on hydromagnetic newtonian liquid flow due to an exponential stretching sheet, Boundary Value Problems 2012 (1) (2012) 1–16.

[30] M. El Kot, W. Abbas, Numerical technique of blood flow through catheterized arteries with overlapping stenosis, Computer Methods in biomechanics and Biomedical Engineering 20 (1) (2017) 45–58.

[31] M. Q. Brewster, Thermal radiative transfer and properties, John Wiley & Sons, 1992.

[32] P. Datti, K. Prasad, M. S. Abel, A. Joshi, Mhd visco-elastic fluid flow over a non-isothermal stretching sheet, International Journal of Engineering Science 42 (8-9) (2004) 935–946.

[33] J. C. Maxwell, A treatise on electricity and magnetism, Vol. 1, Clarendon press, 1873.

[34] P. K. Kambhatla, O. Ojjela, S. K. Das, Viscoelastic model of ethylene glycol with temperature-dependent thermophysical properties, Journal of Thermal Analysis and Calorimetry 135 (2) (2019) 1257–1268.

[35] R. K. Tiwari, M. K. Das, Heat transfer augmentation in a two-sided lid-driven differentially heated square cavity utilizing nanofluids, International Journal of heat and Mass transfer 50 (9-10) (2007) 2002–2018.

[36] M. Sahraoui, M. Kaviany, Slip and no-slip velocity boundary conditions at interface of porous, plain media, International Journal of Heat and Mass Transfer 35 (4) (1992) 927–943.

[37] H. C. Brinkman, The viscosity of concentrated suspensions and solutions, The Journal of chemical physics 20 (4) (1952) 571–571.

[38] T. Hayat, M. Rashid, M. Imtiaz, A. Alsaedi, Mhd effects on a thermo-solutal stratified nanofluid flow on an exponentially radiating stretching sheet, Journal of Applied Mechanics and Technical Physics 58 (2) (2017) 214–223.

[39] J. Kierzenka, L. F. Shampine, A bvp solver that controls residual and error, Journal of Numerical Analysis, Industrial and Applied Mathematics 3 (1-2) (2008) 27–41.

[40] R. Kandasamy, I. Muhaimin, R. Mohammad, Single walled carbon nanotubes on mhd unsteady flow over a porous wedge with thermal radiation with variable stream conditions, Alexandria Engineering Journal 55 (1) (2016) 275–285.

[41] L. F. Shampine, J. Kierzenka, M. W. Reichelt, et al., Solving boundary value problems for ordinary differential equations in matlab with bvp4c, Tutorial notes 2000 (2000) 1–27.

[42] L. F. Shampine, L. F. Shampine, I. Gladwell, S. Thompson, Solving ODEs with matlab, Cambridge university press, 2003.

[43] E. Magyari, B. Keller, Heat and mass transfer in the boundary layers on an exponentially stretching continuous surface, Journal of Physics D: Applied Physics 32 (5) (1999) 577.

[44] D. Srinivasacharya, P. Jagadeeshwar, Effect of joule heating on the flow over an exponentially stretching sheet with convective thermal condition, Mathematical Sciences 13 (3) (2019) 201–211.